Uncertainty quantification of injected droplet size in mono-dispersed Eulerian simulations

Théa Lancien, Nicolas Dumont, Kevin Prieur, Daniel Durox, Sébastien M. Candel, Olivier Gicquel, Ronan Vicquelin

Uncertainty quantification of injected droplet size in mono-dispersed Eulerian simulations

Théa Lancien[1], Nicolas Dumont[1], Kevin Prieur[1,2], Daniel Durox[1], Sébastien Candel[1], Olivier Gicquel[1] and Ronan Vicquelin[1] *

[1] *Laboratoire EM2C, CNRS, CentraleSupélec, Université Paris-Saclay, Grande Voie des Vignes, 92295 Chatenay-Malabry cedex, France*

[2] *Safran Tech, E&P, Rue des Jeunes Bois, Chateaufort, CS 80112, 78772 Magny-Les-Hameaux, France*

Abstract

Large-eddy simulations (LES) of a laboratory-scale two-phase burner are considered by describing the disperse liquid spray with a mono-disperse Eulerian approach. In this simplified framework, the choice of the size of the injected droplets becomes a critical issue. The impact of this key parameter upon the numerical results is carefully assessed though uncertainty quantification tools. Using Polynomial Chaos Expansion and Clenshaw-Curtis nested quadrature rule, several LES are performed for different injected droplet sizes in order to obtain a response surface of velocity and diameter fields at any point in the computational domain as a function of the injected one. Post-treatment of the response surface gives access to the precise impact of the chosen injected droplet size on the results. It is shown that information obtained from different mono-disperse simulations enables to answer a couple of practical questions in such two-phase flow simulations: How can the mono-disperse simulations be compared to the poly-disperse experimental results and their accuracy evaluated? More importantly, if only one simulation is to be carried out for a larger case, which value of the injected droplet size is the best?

Keywords: Two-phase flows, Polynomial Chaos Expansion, Large Eddy Simulation, Eulerian-Eulerian approach

1. Introduction

Reliable and easy ignition constitutes a central issue in the design of practical combustion systems and is specifically important in the case of gas turbines and aero-engines. In the last devices, one complication results from the presence of multiple injection units and a successful ignition process follows then three main stages [14]: (1) A spark is produced by an igniter and leads to the formation of a kernel of hot gases; (2) If the kernel's size and temperature enable its spreading, the corresponding volume increases in a second phase until it reaches the closest fuel injector, thus establishing an initial flame; (3) In the final stage, the flame propagates from burner to burner until a flame is stabilized around each injector. Due to the geometrical complexity of the chamber with its many injectors, this last propagation step, also called light-round, has been less well investigated in the literature than the first two stages. Clearly, a detailed understanding of the ignition process in such systems may be gained by combining well controlled experiments with calculations based on advanced large eddy simulations. One pioneering demonstration of the feasibility of full scale calculations of the light-round in a generic helicopter gas turbine combustor is reported by Boileau et al. [4] but without detailed comparisons with experiments. Detailed ignition experiments in a laboratory-cscale annular combustor (MICCA) operating under premixed conditions [5] have recently provided high speed visualizations of the flame spreading process together with systematic measurements of the ignition delay. Large eddy simulations of this configuration have been successfully compared with further experimental data in [21, 20]. The effect of spacing between injectors was studied in [3] on a linear five-burner configuration. Further experiments under perfectly premixed conditions and gaseous non-premixed conditions are also reported in [16].

However, with the exception of [4], all previous studies were carried out with gaseous flows while aero-engine combustors operate with liquid fuel injected as a spray. Accounting for the presence of the spray of fuel droplets is clearly necessary to be truly representative of ignition in aeronautical gas turbines. It is also worth noting that new data are available for liquid spray injection in the MICCA annular configuration [23] and that these data could be used in comparisons with detailed simulations.

The final objective of this research is to develop such simulations and compare results with these data. The present article is intended to define modeling aspects and it specifically considers questions linked to the modeling of the disperse phase.

Envisioning such large scale simulations with liquid spray injection gives rise to several modeling issues: (i) One is first faced with the problem of describing the spray atomization process. This cannot be included in such calculations and the disperse liquid phase injected in the simulations needs to be modeled; (ii) Second, a compromise has to be found for the description of the polydisperse droplet mist to be consistent with the available computational resources. This issue is considered in what follows. Among the many possible representations, two approaches have been explored in large eddy simulation of two-phase reacting flows. Both rely on a mesoscopic point-particle approximation [9]: The Eulerian-Eulerian approach where moments (see also quadrature-based methods [8]) of the number density function (NDF) are transported [27, 25] and the Eulerian-Lagrangian in which a large ensemble of particles is transported [15, 6, 11]. While accounting for polydispersity in the Eulerian-Lagrangian framework is straightforward, the Eulerian-Eulerian approach requires additional transport equations for moments and/or classes of particle sizes [17, 28]. On the other hand, one of the drawbacks of the Lagrangian methods is the complex handling of computational load balancing on parallel machines for large scale simulations [10]. This issue is expected to become even more problematic in the envisioned light-round simulations where the balance of computational load between ignited and non-ignited injectors needs to be treated dynamically. In order to find the best com-

* This work was supported by grant ANR14-CE23-0009-01 of the French Agence Nationale de la Recherche.

promise between cost and accuracy, under constraints of limited computational resources, the present study explores the possible use of a mono-disperse Eulerian-Eulerian representation of a polydisperse spray. An original feature of the method proposed in this article is that the optimum value of the mono-disperse injected droplets diameter that best represents the evolution of the spray is deduced by computing a surface response on mono-disperse Eulerian simulations thanks to uncertainty quantification (UQ) methodology. This analysis is carried out on a single injector configuration and its result will enable future light-round simulations with a controlled accuracy of the injected droplet diameter.

The single burner investigated experimentally and numerically is presented is section 2. This section also discusses mono-disperse simulation using the spray's Sauter Mean Diameter (SMD). The study of the influence of the injected diameter is then carried out in the uncertainty quantification perspective as detailed in section 3.

2. Mono-disperse Eulerian simulation with the spray Sauter Mean Diameter

2.1. *Experimental setup*

The experimental burner studied is displayed in Fig. 1. The air injected in the system flows through a swirl injector ("G" arrows on the figure) before meeting the n-heptane liquid injector, a simplex atomizer located with a 6 mm recess from the convergent exhaust. The two-phase flow exits the burner into the atmosphere through a diameter $d = 8$ mm with a measured swirl number of 0.68. A Phase Doppler Anemometry system (PDA) is used to measure the gas and droplets velocity profiles as well as the droplets diameter. Measurement were carried out at different distances from the injector exhaust section. The studied operating conditions correspond to air mass flow rate 1.84 g/s and liquid n-heptane mass flow rate 0.11 g/s.

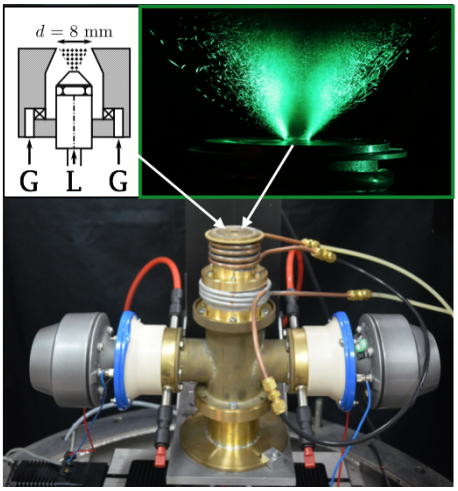

Figure 1: Experimental burner. A sketch of the swirler appears in the top left-hand corner and a vertical tomography of the spray is shown in the top right-hand corner.

Top-right corner Fig.1 shows a tomographic slice of the droplet spray, visualized by means of an argon-ion laser at 514.5 nm. The hollow cone shape of the flow appears clearly, with an inner recirculation zone where few droplets are present. The droplet diameter repartition measured at one point located in the spray (at the radius $r = 4.5$ mm) 2.5 mm above the exhaust plane is presented in Fig. 2. The number distribution spans from $d_l = 0.5$ μm to $d_l = 35$ μm, which shows the polydisperse nature of the spray. The diameter interval corresponds to a range of Stokes number $\tau_p d/U$ of [0, 0.45] where $\tau_p = (1 + 0.15Re_p^{0.687})\frac{\rho_l d_l^2}{18\mu}$ is the droplet's drag characteristic time given the droplet diameter d_l. The evaporation time τ_e expressed in terms of $\tau_e d/U$ corresponds to the range [0.08; 300], which shows that evaporation is reduced for most droplets.

The mean diameter $D_{10} = (\sum_N d)/N$ and the Sauter Mean Diameter $D_{32} = (\sum_N d^3)/(\sum_N d^2)$ are indicated for the considered point ($r = 4.5$ mm, $z = 2.5$ mm) in Fig. 2. With $D_{10} = 8$ μm, the spray is mainly formed by small droplets. In the perspective of combustion, the evaporation rate of the droplets in the polydisperse spray is determined by the spray repartitions in mass and surface [14]. For reactive flow simulations, the Sauter Mean Diameter is usually considered for an equivalent mono-disperse spray simulation that has the same volume to surface ratio as the polydisperse spray. In the present case, $D_{32} = 20$ μm.

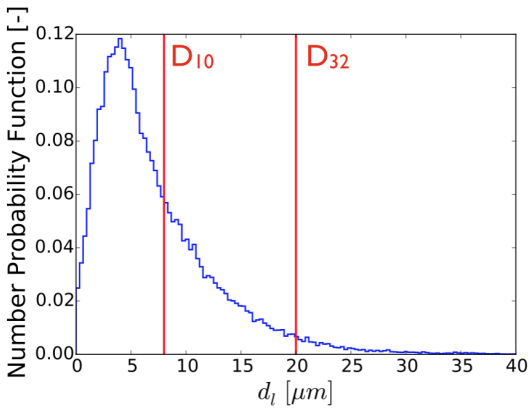

Figure 2: Distribution of droplet diameter in the spray at $x = 2.5$ mm from the exhaust plane and $r = 4.5$ mm.

2.2. *Numerical setup*

Simulations are carried out with the three-dimensional compressible Navier-Stokes solver AVBP [26], jointly developed by CERFACS and IFP Energies Nouvelles. It is based on a centered scheme and uses a two-step Taylor-Galerkin weighted residual central distribution scheme, third order in time and space (TTGC [7]) for both gaseous and liquid phases. The Wall Adapting Local Eddy model (WALE) [19] describes the sub grid scale turbulence. As motivated in the introduction, the numerical description of the liquid disperse phase is a mono-disperse Eulerian approach. The evaporation of the droplets is represented by using the Abramzon-Sirignano model [1]. The computational domain is displayed in Fig. 3. The air guides are included and the ambient air above the burner exhaust plane is taken into account through a large meshed volume. The boundary conditions are standard Navier-Stokes characteristic boundary conditions (NSCBC) [22] and are set according to the experimental parameters. The gas and liquid temperatures are set to 298 K. Initial results are presented for an injected droplet diameter $d_l^{inj} = D_{32} = 20$ μm. All the walls are considered to be adiabatic in the simulations. The mesh counts 17.5 million cells, which corresponds to 3 million nodes. The regions where the highest velocity gradients are found are refined, as well as the area around the liquid injection to deal with high gradients of volume fraction (see Fig. 3). The atmospheric domain where the spray is observed experimentally is also refined in order to capture its dynamics. The mesh is then progressively coarsened until the limits of the domain. A mesh convergence study has demonstrated the adequacy of the retained discretiza-

tion.

The simulation is first run by only injecting the air to establish the gaseous flow. Mean velocity fields are calculated and validated against experimental data. Fuel droplets are then injected in the flow. It is worth noting that the gaseous solution used to initialize the two-phase flow simulations is the same throughout the whole study. After computing a transient physical time equal to several flow-through times, statistical mean fields are computed. Several consecutive average fields are compared to ensure statistical convergence of the velocity field.

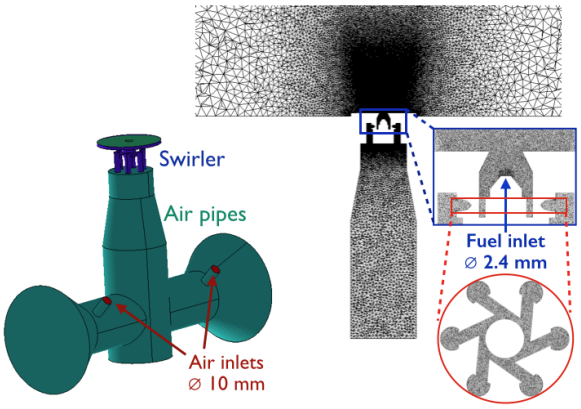

Figure 3: Computational domain for the simulations showing a slice in the mesh. The outer atmospheric domain is not shown.

2.3. *Results*

Gaseous phase velocity

Profiles of the axial and azimutal components of the mean velocity of the gaseous phase are displayed in Fig. 4. The symbols represent the experimental data and the full lines show the numerical results. Data from the purely gaseous case (in black) as well as from the two-phase flow case (in red) are presented. The experimental gaseous flow is nearly identical with or without droplets, which indicates that the diluted disperse liquid phase has little influence on the gaseous phase. For both cases, the simulation is able to retrieve the experimental data with a good accuracy. In particular, the radial position of the recirculation zone is well predicted, and the velocity peak levels are obtained with great accuracy.

Liquid phase velocity

Figure 5 shows the profiles of the mean axial velocity of the liquid phase at an axial distance of $x = 2.5$ mm from the burner exhaust plane. Two different experimental averaged velocities are plotted. The triangles correspond to the arithmetic mean of the droplet's velocity, meaning that every droplet has the same weight in the average, whatever its mass is. The predicted numerical velocity profile does not agree with this type of measurement, which can be explained. On the one hand, as the spray is mainly populated (in number) by small droplets in the experimental setup (see Fig 2), the experimental mean velocity is governed by small droplets dynamics which, having a smaller Stokes number, tend to follow the air flow. On the other hand, the simulated disperse liquid phase corresponds to droplets whose diameter at the injection is equal to the spray's Sauter Mean Diameter $D_{32} = 20\ \mu m$. Because of this larger injected diameter than the majority of droplets, the simulated droplets will have a more ballistic type of trajectory and their velocity relaxes to the gas velocity with a larger characteristic time, which explains the discrepancy between the results.

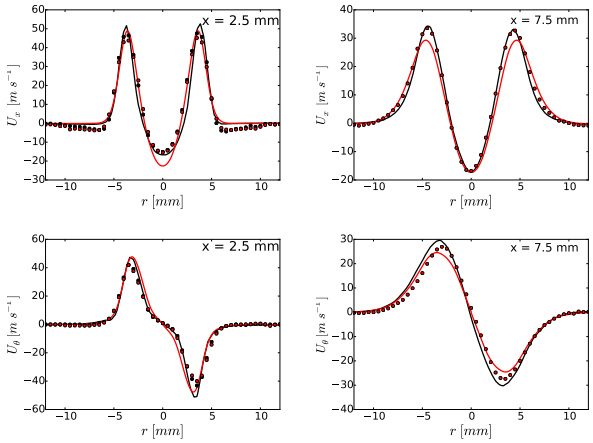

Figure 4: Mean velocity profiles for the gas phase at $x = 2.5$ mm (left) and $x = 7.5$ mm (right) from the exhaust plane: Axial velocity (top) and azimutal velocity (bottom). Black curves represent the results from the gaseous simulation and the red curves the gaseous fields in the two-phase flow simulation. −: Numerical results; • : Experimental data.

In light of these considerations, the numerical fields are compared to the experimental velocities weighted by each particle's mass. Indeed, the final objective of this study is to represent a burning polydisperse spray with a mono-disperse approach, which means describing accurately the spray mass distribution and momentum. Weighting the droplets velocities by their mass seems therefore appropriate. This field is plotted in red in Fig. 5. The numerical results are then much closer to the experimental mass-averaged velocity than they were to the arithmetic average. As with the gaseous fields, the radial position of the spray is well recovered, as well as the magnitude of the peaks. The central recirculation zone that appears in the axial velocity profile is also satisfactorily captured.

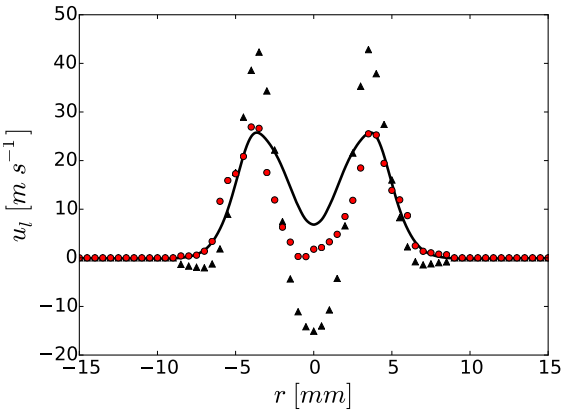

Figure 5: Mean axial velocity for the liquid phase at $x = 2.5$ mm. −: Numerical results; ▲: Experimental arithmetic average; •: Experimental mass-weighted average.

Figure 6 shows the radial profiles for the mean liquid axial velocity, included size-conditioned statistics, at $x = 7.5$ mm in the flame stabilization zone. The full line represents the numerical result, while the experimental mass-averaged velocity is represented in symbols. The dotted lines show the experimental

velocities for several classes of droplets. To ensure experimental convergence, only points where enough data (more than 100 droplets) have been collected are plotted. Comparing the different experimental fields, it appears that the different droplet classes behave quite similarly with a spreading due to the different drag relaxation time. This similarity leads to the mass-averaged field being quite close to the arithmetic average (not shown), which was not the case at $x = 2.5$ mm. Indeed, the measurement plane $x = 7.5$ mm being further away from the burner exhaust plane, the bigger droplets have had more time to relax towards a more uniform flow. Figure 4 showed that the gaseous velocity field was very well predicted. However, some discrepancies appear for the liquid phase fields. First of all, only very small droplets are present in the center recirculation zone in the experiment, whereas the numerical 20 μm droplets are not sensitive to the same entrainment effect in the center recirculation zone, which is not retrieved then by the simulation. Looking at the two high velocity peaks indicates that, though the simulations is very accurate in predicting the gaseous peaks as well as the radial position of the spray, it is not able to retrieve the correct magnitude of the average liquid velocity. The larger droplets that are numerically resolved are not sufficiently entrained by the air flow to be representative of the mass-weighted liquid velocity. The numerical profile is however closer to the experimental 20 μm-class velocity (in red), indicating that, while the injected droplets do not behave like the average of the spray, their dynamics matches the corresponding experimental class.

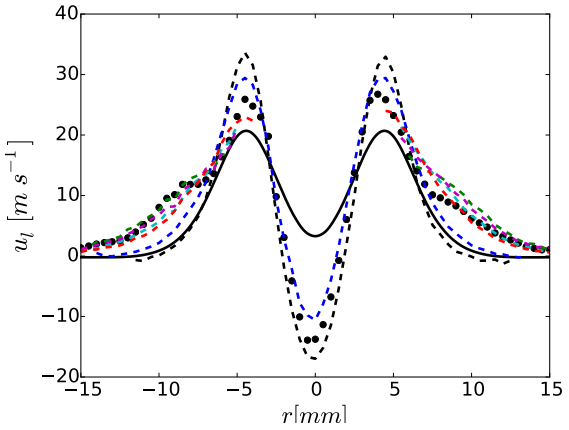

Figure 6: Mean axial velocity field for the liquid phase at $x = 7.5$ mm. −: Numerical results; •: Mass-averaged experimental field; Experimental profiles: - -: $d_l = 2-3\ \mu m$; - -: $d_l = 10-12\ \mu m$; - -: $d_l = 20-23\ \mu m$; - -: $d_l = 23-36\ \mu m$; - -: $d_l = 26-30\ \mu m$. - -: $d_l = 30-34\ \mu m$;

Consequently, although the general behavior of the two-phase flow is retrieved qualitatively, the single simulation of a mono-disperse spray with $d_l^{inj} = D_{32}$ is not able to accurately predict the magnitude of the mean velocity fields of a polydisperse spray, which is not surprising. However, if one focuses on the corresponding experimental class of droplet, the simulation is in fair agreement with its evolution. In light of these observations, considering the mono-disperse description as a surrogate model of the polydisperse spray, an optimal injected diameter should be determined in order to retrieve a spray dynamics representative of the experimental one.

3. Uncertainty quantification of the injected droplet size

3.1. *Surface response computation*

An interesting approach in order to evaluate the impact of one or several parameters on a complex system is uncertainty quantification and the Polynomial Chaos Expansions (PCE) [29, 24]. Indeed, PCE allow to approach uncertain fields that depend on both deterministic and uncertain parameters. A given field u can then be written as $u(x, \omega)$ where x represents the deterministic parameters and ω the uncertain ones. In the present study the injected diameter d_l^{inj} is considered to be the unique uncertain parameter. Through PCE, one is able to estimate any given field with the polynomial decompositon:

$$u(x_j, d_l^{inj}) \approx \sum_{k=0}^{N} a_k(x_j) P_k(d_l^{inj}) \tag{1}$$

For any given point x_j, knowing the value of the coefficients $a_k(x_j)$, $u(x_j, d_l^{inj})$ becomes a continuous function of the uncertain parameter d_l^{inj}, whose study is then straightforward. Using non-intrusive methods, the computation of the coefficients $a_k(x_j)$, which are defined by integrals, is carried out with nested quadrature rules: $M = 2^l + 1$ evaluations of $u(x_j, d_l^{inj})$ are required for the l-quadrature level. In the context of LES, several simulations, corresponding to different values of d_l^{inj} are then performed. The retained Clenshaw-Curtis nested quadrature rule enables to limit the number of evaluations for several quadrature levels [12], which is a great benefit given the computational cost of carrying out several large-eddy simulations. The considered injected diameter distribution is considered uniform between 0.5 μm and 35 μm. Due to the cost of each simulation, the maximum quadrature level was limited to 3 for this study. According to the Clenshaw-Curtis quadrature rule, the different values of d_l^{inj} to simulate are presented in table 1: nine large-eddy simulations have been performed in total.

The PCE is here used to build a response surface of LES results in terms of d_l^{inj}. Each field can therefore be estimated by the polynomial approximation for any value of the injected diameter, even one that was not simulated. This provides a way to determine an optimal diameter more efficiently than by carrying out a parametric study with a finite set of values.

3.2. *Analysis of results*

Once all the LES statistics have converged and the averaged fields have been recovered, response surfaces can be reconstructed. At a given point in space and for a given physical field, the polynomial reconstruction yields the variation of this field according to the injection diameter. An example of response surface is given in Fig. 7 for the liquid velocity. Figure 8 gives the response curves of the axial liquid velocity at $x = 7.5$ mm for four different values of the radial coordinate r. Polynomial chaos expansions with different truncation level corresponding to different polynomial degrees are shown along with the LES values (symbols) for the nine considered simulations. Good approximation is achieved from polynomial degrees of four and above. Some oscillations appear at the degree 6 (in magenta), which leads to selecting the degree 5 (in cyan) for further analysis. All PCE results correspond to the 3rd quadrature level. The other quadrature levels (lines #1 and #2 in Tab. 1) enable to check the numerical convergence of the presented results.

Table 1: Values of the injected diameter

Quadrature level	Injected diameter [μm]								
1	0.5	-	-	-	17.75	-	-	-	35.0
2	0.5	-	5.55	-	17.75	-	29.95	-	35.0
3	0.5	1.81	5.55	11.15	17.75	24.35	29.95	33.69	35.0

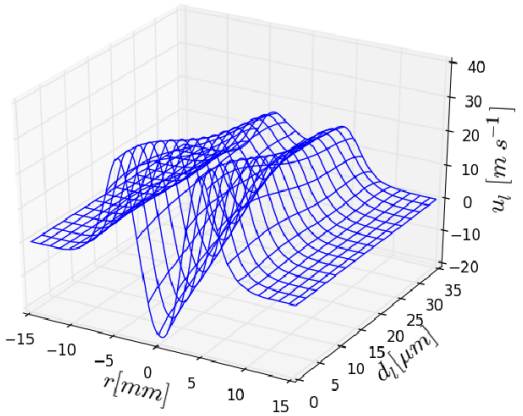

Figure 7: Response surface for the axial velocity at $x = 7.5$ mm and some of the numerical fields used for the expansion.

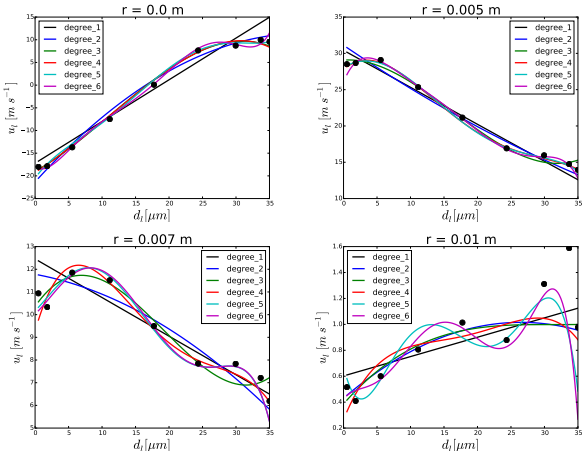

Figure 8: PCE approximation for the axial velocity at $r = 0$ mm (top left), $r = 5$ mm (top right), $r = 7$ mm (bottom left) and $r = 10$ mm (bottom right). $-$: PCE expansions; $\bullet$: Numerical values from mono-disperse simulations.

3.3. *Optimization of the injected diameter*

The response surfaces can be built for any quantity of interest. In order to determine a best value for the injection diameter, it is necessary to define one or several criteria. A first optimization criterion can be the minimization of numerical error on the mass-weighted axial liquid velocity u_{exp}^{poly}. This error criterion, denoted by $||u_l^{mono}(d_l^{inj}) - u_{l,exp}^{poly}||_2$, is defined here for a given height x as

$$\sqrt{\frac{1}{N_{exp}} \sum_{N_{exp}} (u_l^{pce}(r_j, d_l^{inj}) - u_{exp}^{poly}(r_j))^2}, \tag{2}$$

where u_l^{pce} is the response surface of axial liquid velocity obtained in mono-disperse simulations and r_j corresponds to the N_{exp} experimental points at the considered height. The black curve in Fig. 9 shows the relative error norm according to the selected injection diameter. An optimal value for the injected diameter clearly appears at $d_l^{inj} = 9.7\mu$m for this criterion.

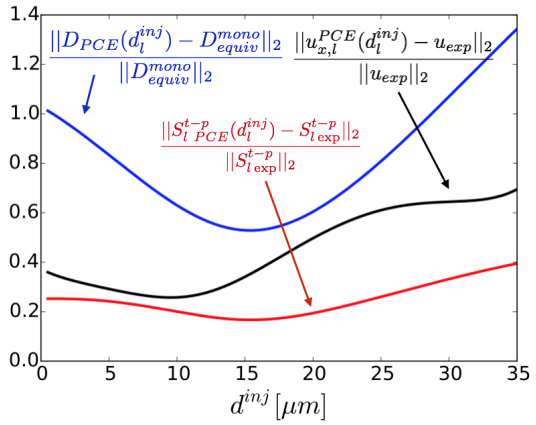

Figure 9: Normalised L^2-norm of both criteria at $x = 7.5$ mm.

The final objective being reactive simulations of flame propagation in a two-phase flow, a key quantity is the laminar burning speed, to consider here in the presence of droplets. Ballal and Lefebvre [2] gave an expression for such a two-phase laminar flame speed S_l^{t-p}, whose validity has been investigated numerically in [18]:

$$S_l^{t-p} = \alpha_g \left[\frac{C_3^3 \rho_l D_{32}^2}{8 C_1 \rho_g \ln(1+B)} + \frac{\alpha_g^2}{S_L^2} \right]^{-0.5} \tag{3}$$

with α_g the thermal conductivity, ρ_l and ρ_g the liquid and gaseous densities, B the Spalding number and S_L the gaseous laminar flame speed. This formula is valid for a polydisperse spray, with $C_1 = D_{20}/D_{32}$ and $C_3 = D_{30}/D_{32}$. In the case of a mono-disperse spray, the coefficients C_1 and C_3 are both equal to unity, which yields the equivalent mono-disperse diameter that conserves the two-phase laminar burning speed:

$$D_{equiv}^{mono} = D_{32}^{poly} \times \sqrt{\frac{C_3^3}{C_1}} \tag{4}$$

The predicted diameter can then be compared to the equivalent one with respect to the flame speed defined in Eq. 4, which is displayed in blue in Fig. 9, again using the relative error norm. The corresponding error on S_l^{t-p} is given in red. It appears that the optimal diameter varies strongly depending on the criterion used. In order to retrieve the liquid velocity fields, injecting small droplets, with a diameter around 9.5 μm, which is close to the spray's mean diameter D_{10}, seems optimal. However, to reproduce the flame speed, a better injection diameter would be around 15.3 μm. For this diameter, the relative error on the flame speed is of 16%, which remains noticeable. These results are consistent with the definition of the diameters given by Lefebvre in [13],

who states that among a set of available representative diameters, the D_{10} represents the velocity fields while the D_{32} is more suited for combustion. However, in order to reduce even more the error on the flame speed, a finer optimization would be required, for example on the actual position of the flame front, which is unknown in the present case.

4. Conclusion

The present investigation is carried out as a first stage preparation of a large scale simulation of the light-round ignition process in a full annular combustor. The objective is to complete the calculation of such a system comprising multiple injectors fed with liquid fuel. One central issue in such simulations is that of the modeling of the liquid droplet spray. It is considered that such a large scale simulation cannot accommodate models which account for the spray polydispersity and that it is interesting to use a mono-disperse Eulerian framework to reduce the computational intensity and comply with limitations in CPU resources. It is next indicated that the droplet size of the spray becomes a key parameter that is here adjusted by making use of an uncertainty quantification framework. This novel method is explored in the case of a single injector investigated experimentally and numerically. Several mono-disperse Eulerian simulations are performed in order to study the impact of the mono-disperse simplification when modeling a polydisperse spray. It is shown that this approach provides a reasonable description of the spray formed in the single injector configuration. The optimal choice of a droplet diameter is then based on the response surface obtained by polynomial chaos expansion and varies with the purpose of the simulation, and therefore the accuracy criterion.

This study relies on the hypothesis that the classes behave in an independent manner. This hypothesis was not validated, which would require a reference simulation using the polydisperse Lagrangian formalism. The inter-class interactions would then be quantified. In order to further validate the optimal injection diameter as well as the criterion used to select it, a simulation with combustion would also be necessary. This will be included in some future work.

References

[1] B. Abramzon and W.A. Sirignano. Droplet vaporization model for spray combustion calculations. *Int. Journal of Heat and Mass Transfer*, 32(9):1605 – 1618, 1989.

[2] D.R. Ballal and A.H. Lefebvre. Flame propagation in heterogeneous mixtures of fuel droplets, fuel vapor and air. *Int. Symposium on Combustion*, 18(1):321 – 328, 1981.

[3] D. Barré, L. Esclapez, M. Cordier, E. Riber, B. Cuenot, G. Staffelbach, B. Renou, A. Vandel, L.Y.M. Gicquel, and G. Cabot. Flame propagation in aeronautical swirled multi-burners: Experimental and numerical investigation. *Combustion and Flame*, 161(9):2387 – 2405, 2014.

[4] M. Boileau, G. Staffelbach, B. Cuenot, T. Poinsot, and C. Bérat. Les of an ignition sequence in a gas turbine engine. *Combustion and Flame*, 154(1–2):2 – 22, 2008.

[5] J.-F. Bourgouin, D. Durox, T. Schuller, J. Beaunier, and S. Candel. Ignition dynamics of an annular combustor equipped with multiple swirling injectors. *Combustion and Flame*, 160(8):1398 – 1413, 2013.

[6] M. Chrigui, J. Gounder, A. Sadiki, A. R. Masri, and J. Janicka. Partially premixed reacting acetone spray using les and fgm tabulated chemistry. *Combustion and Flame*, 159(8):2718–2741, 8 2012.

[7] O. Colin and M. Rudgyard. Development of high-order taylor–galerkin schemes for les. *Journal of Computational Physics*, 162(2):338 – 371, 2000.

[8] R. Fan, D. L. Marchisio, and R. O. Fox. Application of the direct quadrature method of moments to polydisperse gas–solid fluidized beds. *Powder Technology*, 139(1):7–20, 1 2004.

[9] R. O. Fox. Large-Eddy-Simulation Tools for Multiphase Flows. In Davis, SH and Moin, P, editor, *Annual Review of Fluid Mechanics*, volume 44, pages 47–76. Davis, SH and Moin, P, 2012.

[10] M. Garcia. *Development and validation of the Euler-Lagrange formulation on a parallel and unstructured solver for large-eddy simulation*. PhD thesis, Institut National Polytechnique de Toulouse, 2009.

[11] W. P. Jones, S. Lyra, and S. Navarro-Martinez. Numerical investigation of swirling kerosene spray flames using large eddy simulation. *Combustion and Flame*, 159(4):1539–1561, 4 2012.

[12] M. Khalil, G. Lacaze, J. C. Oefelein, and H. N. Najm. Uncertainty quantification in les of a turbulent bluff-body stabilized flame. *Proceedings of the Combustion Institute*, 35(2):1147–1156, 2015.

[13] A.H. Lefebvre. *Atomization and Sprays*. Taylor and Francis, 1989.

[14] A.H. Lefebvre and D. R. Ballal. *Gas Turbine Combustion*. Taylor and Francis, 2010.

[15] K. Luo, H. Pitsch, M. G. Pai, and O. Desjardins. Direct numerical simulations and analysis of three-dimensional n-heptane spray flames in a model swirl combustor. *Proceedings of the Combustion Institute*, 33(2):2143–2152, 2011.

[16] E. Machover and E. Mastorakos. Spark ignition of annular non-premixed combustors. *Experimental Thermal and Fluid Science*, 73:64–70, 5 2016.

[17] M. Massot. *Multiphase Reacting Flows: Modelling and Simulation*, chapter Eulerian Multi-Fluid Models for Polydisperse Evaporating Sprays, pages 79–123. Springer Vienna, 2007.

[18] A. Neophytou and E. Mastorakos. Simulations of laminar flame propagation in droplet mists. *Combustion and Flame*, 156(8):1627 – 1640, 2009.

[19] F. Nicoud and F. Ducros. Subgrid-scale stress modelling based on the square of the velocity gradient tensor. *Flow, Turbulence and Combustion*, 62(3):183–200, 1999.

[20] M. Philip, M. Boileau, R. Vicquelin, E. Riber, T. Schmitt, B. Cuenot, D. Durox, and S. Candel. Large eddy simulations of the ignition sequence of an annular multiple-injector combustor. *Proceedings of the Combustion Institute*, 35(3):3159 – 3166, 2015.

[21] M. Philip, M. Boileau, R. Vicquelin, T. Schmitt, D. Durox, J.-F. Bourgouin, and S. Candel. Simulation of the ignition process in an annular multiple-injector combustor and comparison with experiments. *Journal of Engineering for Gas Turbines and Power*, 137(3):031501–031501, 09 2014.

[22] T.J Poinsot and S.K Lele. Boundary conditions for direct simulations of compressible viscous flows. *Journal of Computational Physics*, 101(1):104 – 129, 1992.

[23] K. Prieur, D. Durox, J. Beaunier, T. Schuller, and S. Candel. Ignition dynamics in an annular combustor for liquid spray and premixed gaseous injection. *Submitted, Proceedings of the Combustion Institute*, 2016.

[24] M. T. Reagana, H. N. Najm, R. G. Ghanem, and O. M. Knio. Uncertainty quantification in reacting-flow simulations through non-intrusive spectral projection. *Combustion and Flame*, 132(3):545–555, 2003.

[25] M. Sanjosé, J. M. Senoner, F. Jaegle, B. Cuenot, S. Moreau, and T. Poinsot. Fuel injection model for euler–euler and euler–lagrange large-eddy simulations of an evaporating spray inside an aeronautical combustor. *Int. Journal of Multiphase Flow*, 37(5):514–529, 6 2011.

[26] T. Schönfeld and M. Rudgyard. Steady and unsteady flow simulations using the hybrid flow solver avbp. *AIAA Journal*, 37(11):1378–1385, 2016/02/17 1999.

[27] J. M. Senoner, M. Sanjosé, T. Lederlin, F. Jaegle, M. García, E. Riber, B. Cuenot, L. Gicquel, H. Pitsch, and T. Poinsot. Eulerian and lagrangian large-eddy simulations of an evaporating two-phase flow. *Comptes Rendus Mécanique*, 337(6–7):458–468, 2009.

[28] A. Vié, F. Laurent, and M. Massot. Size-velocity correlations in hybrid high order moment/multi-fluid methods for polydisperse evaporating sprays: Modeling and numerical issues. *Journal of Computational Physics*, 237:177–210, 3 2013.

[29] D. Xiu and G. E. Karniadakis. The wiener–askey polynomial chaos for stochastic differential equations. *SIAM journal on scientific computing*, 24(2):619–644, 2002.